Hierarchical carbon composite nanofibrous electrode material for high-performance aqueous supercapacitor

By: Alex Abogaye, Yiyang Liu, James G. Ryan, Jianjun Wei, and Lifeng Zhang

A. Aboagye, Y. Liu, J. Ryan, J. Wei, L. Zhang, Hierarchical carbon composite nanofibrous electrode material for high-performance aqueous supercapacitor, *Materials Chemistry and Physics*, **2018**, 214, 557-563. https://doi.org/10.1016/j.matchemphys.2018.05.009.

Abstract:

In this research, a hierarchical carbon composite nanomaterial ECNFs/PtNPs, which is composed of electrospun carbon nanofibers (ECNFs) with both individual and agglomerate of Pt nanoparticles (PtNPs) homogeneously dispersed all over the ECNF surface, was prepared by successive electrospinning, carbonization, and controlled growth of the PtNPs. Morphology and structure of ECNFs and ECNFs/PtNPs with a variety of amount of PtNPs were characterized by scanning electron microscope, x-ray diffraction and BET surface area analysis. The ECNFs/PtNPs was evaluated as electrode material for supercapacitor with aqueous electrolyte. The results indicated that Pt nanoparticles on surface of ECNFs drastically increased specific capacitance as well as potential energy density of the electrode material by 50 times to 226 F g^{-1} and 20 W h kg^{-1}, respectively, at 0.14 g/cm^2 Pt loading with 6M KOH aqueous electrolyte. This is ascribed to the highly catalytic activity of PtNPs in the hierarchical nanostructure for oxygen reduction reaction in alkali aqueous electrolyte, which leads to significant pseudocapacitance. This research discloses a novel nanofibrous electrode material from electrospinning with great potential for designing high-performance supercapacitors using aqueous electrolyte.

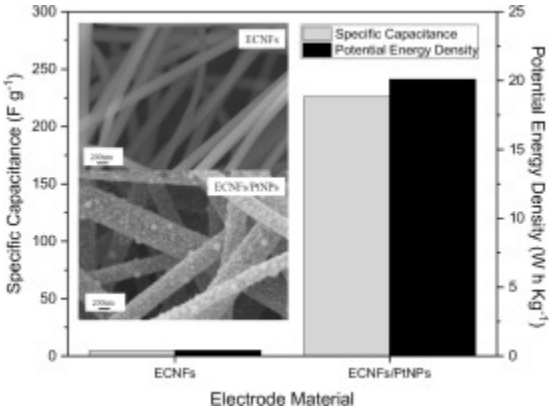

Keywords: Supercapacitor | Carbon nanofibers | Pt nanoparticles | Oxygen reduction reaction Pseudocapacitance

1. Introduction

In recent years, supercapacitor technology has undergone considerable research and development due to its high capacitance that bridges the gap between batteries and conventional capacitors [1]. Supercapacitors provide higher energy density than conventional capacitors and much higher power density than batteries. As a result, supercapacitors are often used in stationary and mobile systems that require high-power pulses such as car acceleration, tramways, cranes, forklifts, emergency and power back-up systems, and so on. Based on mechanism of charge storage, supercapacitors can be categorized into three general classes: electrochemical double-layer capacitors (EDLCs), pseudocapacitors, and hybrid capacitors. EDLCs store charges at interface between electrode and electrolyte as voltage is applied. In EDLCs, accumulation of charges at electrode is a non-Faradaic process and there is no charge transfer between electrode and electrolyte. Increase of surface area as well as decrease of electrode distance makes it possible for EDLCs to achieve higher energy densities than conventional capacitors [2,3]. EDLCs are able to provide ultrahigh power and outstanding cycle life due to fast and non-degradation process between electrode active material and electrolyte [4]. Pseudocapacitors make use of fast and reversible redox reaction to store electrical charges [5,6]. Accumulation of electrons at electrode in pseudocapacitors is a Faradaic process where the electrons generated by a redox reaction are transferred across the electrode-electrolyte interface. Pseudocapacitors can attain greater capacitances and energy densities than EDLCs but their power performance is usually lower than that of EDLCs [7]. Hybrid capacitors utilize both Faradaic and non-Faradaic processes to store charges. They exhibit improved performance because they exploit the advantages and mitigate the disadvantages of EDLCs and pseudocapacitors [8,9].

The characteristic of electrode material is the most critical factor that governs the performance of supercapacitors [10]. Carbon material has been choice of electrode material for supercapacitors because of their excellent electrical conductivity and chemical stability. Electrospun carbon nanofibers (ECNFs) have been reported as promising electrode material for supercapacitors because high aspect ratio of nanofibers enables formation of a conductive network which facilitates charge transfer and in the meantime they can be used directly as free-standing and binder-free electrode [11]. To improve specific capacitance and energy density of ECNFs based supercapacitors, the most popular way is to increase specific surface area of ECNFs [11,12] and/or reduce their charge transfer resistance by adding graphene nanosheets to facilitate its EDLC specific capacitance [13,14]. To further increase specific capacitance of supercapacitors, transition metal oxides are being investigated as coating on ECNFs surface where metal oxide acts as redox center and both EDLC and pseudo-capacitance can be simultaneously generated to form a hybrid supercapacitor [15]. For example, MnO_2 is one of the best candidate materials for pseudo-capacitor electrode because it has high theoretical specific capacitance ($\sim$1380 F g^{-1}) in addition to environmental friendliness and low cost. Unfortunately poor electrical conductivity of metal oxide limits its full utilization for practically high pseudo-capacitance.

Recently ECNFs with surface-attached Pt nanoparticles have served as counter electrode in dye-sensitized solar cells where they demonstrated significantly higher electro-catalytic performance

in I^-_3 reduction reaction at interface between counter electrode and electrolyte as well as smaller charge transfer resistance [16]. This hierarchical nanomaterial may also have potential as electrode material for supercapacitors due to good electrical conductivity and catalytic capacity of Pt metal nanoparticles in the case that Faradic process happens, which may significantly improve its pseudo-capacitance. In this study, ECNFs and ECNFs with a variety of amounts of Pt nanoparticles on surface were explored for the first time as electrode material aiming at high pseudo-capacitance. The results indicated that Pt nanoparticles on surfaces of ECNFs drastically increased specific capacitance of the supercapacitor with alkali aqueous electrolyte through oxygen reduction reaction. This research disclosed a potential electrode nanomaterial for high-performance supercapacitors using alkali aqueous electrolyte.

2. Experimental

2.1. Materials

Polyacrylonitrile (PAN, Mw = 150 kDa), N, N-dimethylformamide (DMF), chloroplatinic acid (H_2PtCl_6), and formic acid (HCOOH) were purchased from Sigma-Aldrich (St. Louis, MO) and used as received without further purification.

2.2. Preparation of electrospun carbon nanofibers (ECNFs) with surface-decorated Pt nanoparticles (ECNFs/PtNPs)

ECNFs were prepared by electrospinning a PAN solution followed by stabilization and carbonization according to our previous report [16]. A 2 in. × 2 in. ECNFs mat was first sonicated and then placed in a solution that was composed of 400 ml chloroplatinic acid (H_2PtCl_6, the Pt precursor) and 40 ml formic acid (HCOOH, the reducing reagent). The reaction system was maintained at room temperature for 48 h to complete reduction of H_2PtCl_6. The product was then washed several times with deionized water and dried at room temperature afterwards. Three types of ECNFs/PtNPs were prepared at H_2PtCl_6 concentrations of 0.5 mM, 1 mM, and 1.5 mM and correspondingly labeled as ECNFs/PtNPs-1, ECNFs/PtNPs-2, and ECNFs/PtNPs-3, respectively. Each sample before and after PtNPs growth was weighted. Pt loading was defined as percentage of weight increase with respect to original mass of ECNFs.

2.3. Characterization

Surface morphology and structure of ECNFs and ECNFs/PtNPs electrode materials were examined by a Carl Zeiss Auriga-BU FIB field emission scanning electron microscope (FESEM). Specific surface area, pore volume and pore size of these electrode materials were determined by nitrogen adsorption using a surface area and pore analyzer (Micromeritics ASAP 2020, Norcross, GA). X-ray diffraction patterns of these electrode materials were obtained using a Bruker D8 X-ray Diffractometer.

Electrochemical performance evaluation of the electrode materials of ECNFs and ECNFs/PtNPs was carried out on an electrochemical workstation (BioLogic VMP3) using a three-electrode testing system in 6M KOH electrolyte solution. In this three-electrode setup, a 5 mm × 5 mm square piece of electrode material was adhered to a gold electrode using carbon glue and worked

as working electrode while a platinum wire worked as counter electrode and Ag/AgCl/KCl (3M) worked as reference electrode (~0.210 V vs. SHE). Cyclic voltammetry (CV) was collected at different scan rates with a potential window of −0.5-0.3 V vs. Ag/AgCl/KCl (3M). Galvanostatic charge/discharge test was done at current density of 4,320 mA g^{-1}.

3. Results and discussion

3.1. Morphology and structure

Typical fiber shape and smooth surface were observed for ECNFs with an average diameter of ~300 nm (Fig. 1). Amount and size of Pt nanoparticles on surface of ECNFs/PtNPs increased with Pt precursor concentration in solution. Sporadic Pt nanoparticles with sizes of a few tens of nanometers were observed on fiber surface of ECNFs/PtNPs-1 and ECNFs/PtNPs-2. Both individual Pt nanoparticles as well as agglomerate of Pt nanoparticles with sizes in the range of tens to hundreds of nanometers were largely observed and distributed homogeneously on fiber surface of ECNFs/PtNPs-3.

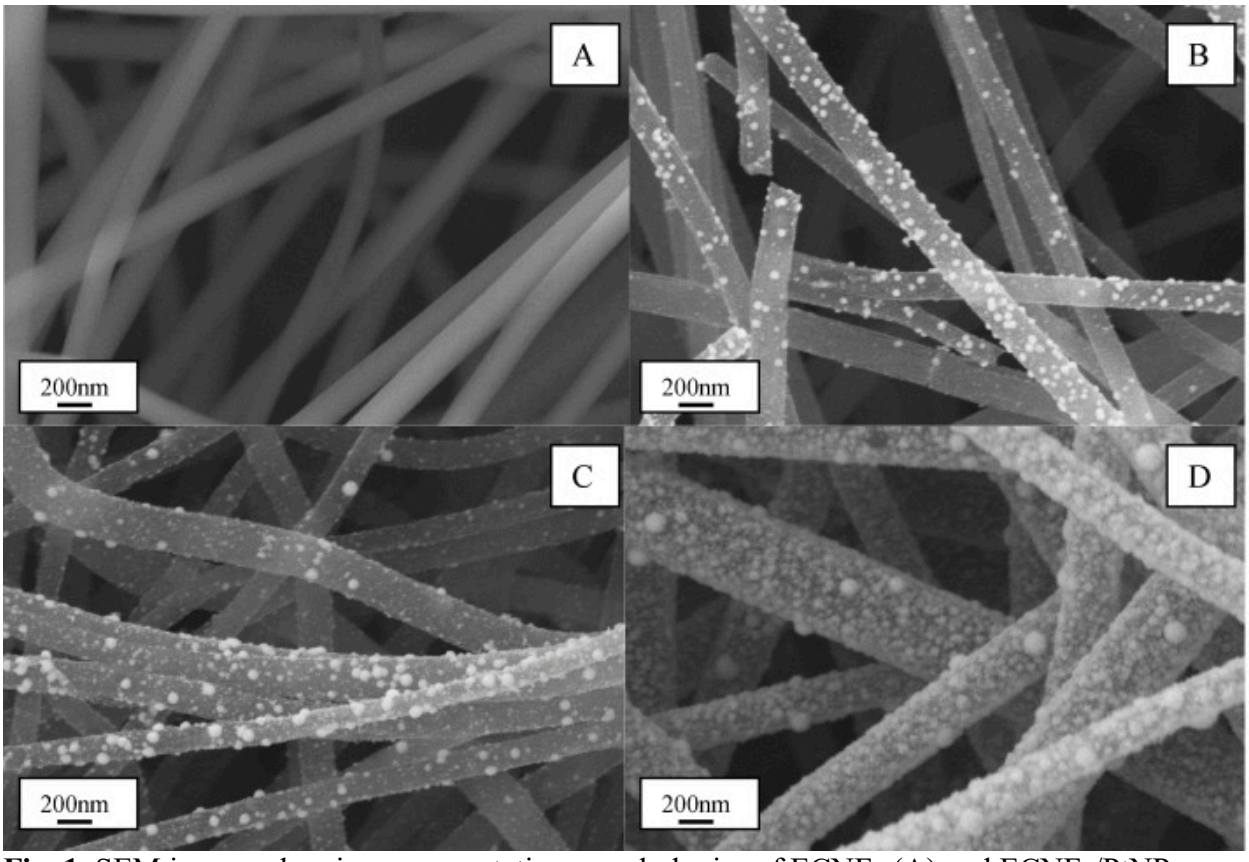

Fig. 1. SEM images showing representative morphologies of ECNFs (A) and ECNFs/PtNPs from 0.5 mM (B), 1.0 mM (C), and 1.5 mM (D) Pt precursor solutions.

Loading of Pt nanoparticles of three ECNFs/PtNPs samples were ~10 wt%, ~40 wt% and ~110 wt% with respect to ECNFs weight, which are equivalent to 0.028, 0.052, 0.14 g Pt per square centimeter electrode, respectively. XRD patterns of the ECNFs and ECNFs/PtNPs

samples are shown in Fig. 2. Three diffraction peaks centered at 2θ angles of 39.87°, 46.25°, and 67.75°, which correspond to (1 1 1), (2 0 0) and (2 2 0) crystallographic planes of face centered cubic (fcc) crystal structure of Pt, respectively, were observed for ECNFs/PtNPs samples and confirmed presence of Pt metal nanoparticles on ECNFs.

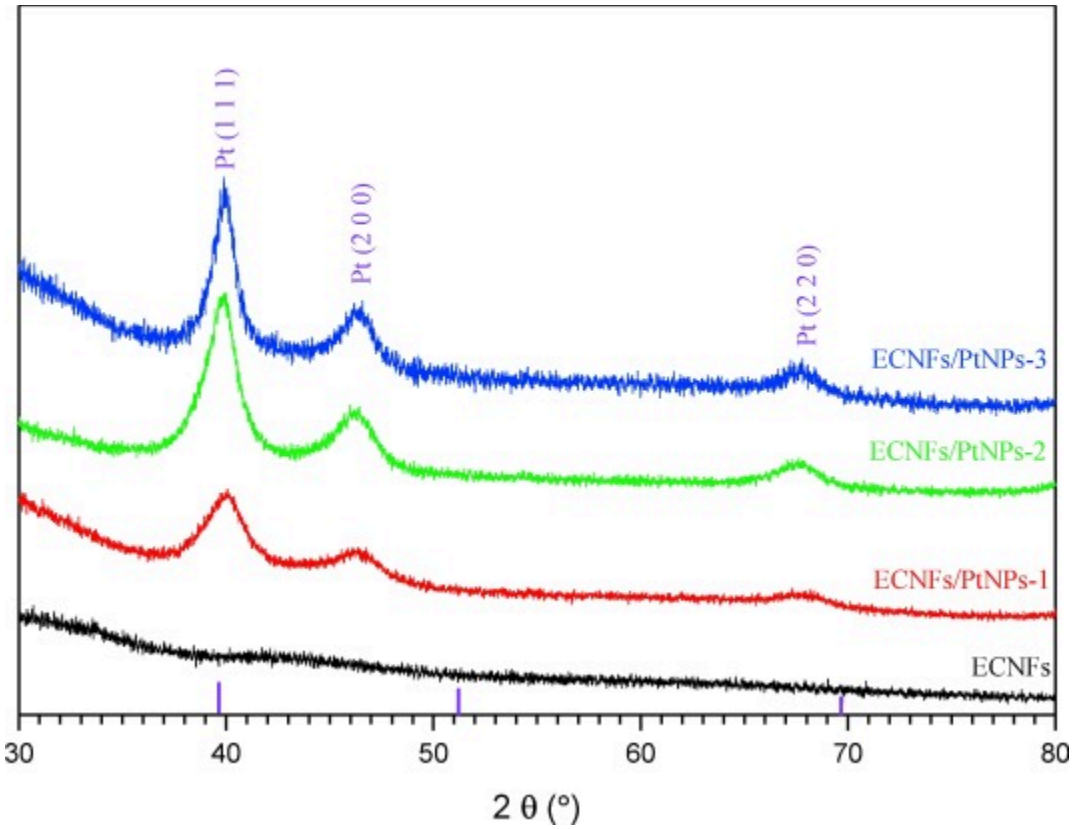

Fig. 2. XRD patterns of ECNFs and ECNFs/PtNPs.

Table 1. Specific surface area, volume and pore size of ECNFs and ECNFs/PtNPs electrode materials.

Sample	BET Specific Surface Area ($m^2\ g^{-1}$)	Average Pore Size (Å)	Pore Volume ($cm^3\ g^{-1}$)
ECNFs	11	86	0.0244
ECNFs/PtNPs-1	15	162	0.0362
ECNFs/PtNPs-2	15	129	0.0451
ECNFs/PtNPs-3	17	101	0.0610

Pristine ECNFs have a BET specific surface area (SSA) of ~11 $m^2\ g^{-1}$ while a theoretical value based on the assumption of cylindrical solid carbon fiber with 300 nm diameter is approximately 6 $m^2\ g^{-1}$, indicating some porous structure inside the prepared ECNFs (Table 1). Growth of Pt nanoparticles on ECNFs increased overall BET SSA of the resultant hierarchical nanomaterial by 34.0%, 34.5%, and 54.1% for ECNFs/PtNPs-1, ECNFs/PtNPs-2, and ECNFs/PtNPs-3, respectively. Generally speaking, deposition of Pt nanoparticles on the surfaces of ECNFs increases surface area of ECNFs. The overall specific surface area of ECNFs/PtNPs, however, depends on number of individual nanoparticles and/or agglomerates. Larger number of Pt nanoparticles ensures higher specific surface area. Higher concentration of Pt precursor is essentially able to generate more Pt nuclei in unit time in the process of nucleation and growth of

PtNPs and the highest specific surface area was thus observed with ECNFs/PtNPs-3. Larger number as well as stacking of Pt nanoparticles led to smaller pore size but more pore volume. The BET SSA data of ECNFs/PtNPs-3 are consistent with corresponding SEM images (Fig. 1D).

3.2. Electrochemical evaluation

Electrochemical performance of the ECNFs and ECNFs/PtNPs electrode materials was evaluated by cyclic voltammetry (CV) and galvanostatic charge/discharge. Typical CV curves of ECNFs and ECNFs/PtNPs electrodes were collected at a scan rate of 5 mV s^{-1} within a potential window from −0.5 V to 0.3 V in 6M KOH aqueous electrolyte (Fig. 3).

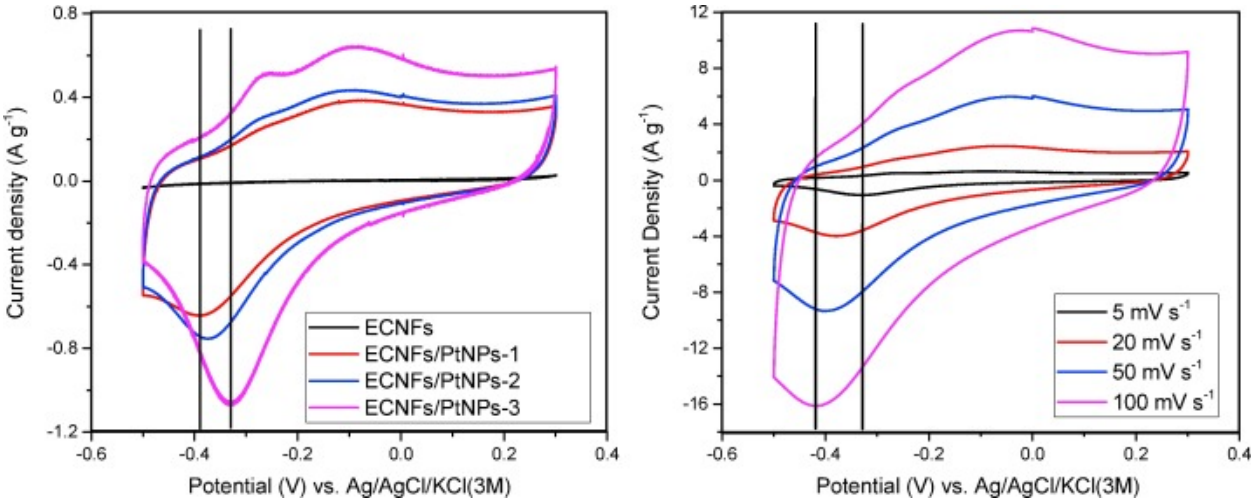

Fig. 3. Cyclic voltammograms (CV) of ECNFs and ECNFs/PtNPs with varying amount of PtNPs at a scan rate of 5 mV s^{-1} (left) and CV of ECNFs/PtNPs-3 at varied scan rate from 5 to 100 mV s^{-1} in 6 M KOH aqueous electrolyte (right).

At scan rate of 5 mV s^{-1}, CV curve of the pristine ECNFs exhibited a long and narrow non-rectangular shape and enclosed very small area of loop, suggesting very small electrochemical double layer capacitive behavior. In the meantime, no significant redox peaks was observed. CV curves of the ECNFs/PtNPs enclosed much larger area of loop and the area increased with PtNPs loading, indicating much higher specific capacitance for ECNFs/PtNPs. Significant redox peaks in the range of −0.3 V to −0.4 V (vs. Ag/AgCl/KCl(3M)) were observed for ECNFs/PtNPs electrode materials. With the increase of Pt loading, the reduction peak shifts toward positive direction from −0.388 V to −0.329 V and reduction current density increases significantly from 0.641 A g^{-1} to 1.058 A g^{-1}, indicating much easier reduction reaction. With the increase of scan rate, CV loops of ECNFs/PtNPs-3 enclosed much larger area of loop and became more rectangular. The redox peak shifted toward negative direction from −0.329 V to −0.421 V (vs. Ag/AgCl/KCl(3M)) and reduction current density significantly increased from 1.058 A g^{-1} to 16.135 A g^{-1}.

Specific capacitance of the ECNFs and ECNFs/PtNPs electrode materials was obtained from CV curves using the equation (1) shown below [17,18].

$$C = \frac{\int_{V_a}^{V_c} I(V)dV}{\omega v(V_c - V_a)} \quad (1)$$

where *C* is specific capacitance of electrode material; ω is mass of active constituent in working electrode; *v* is the potential scan rate; V_c–V_a is sweeping potential window; and I(V) is current density.

Specific capacitance of the ECNF and ECNF/PtNPs electrode materials was calculated based on the CV curves at 5 mV s^{-1} (Fig. 4). The specific capacitance of pure ECNFs was 4.6 F g^{-1}. The specific capacitance values significantly increased as the PtNPs were introduced on surface of the ECNFs. The specific capacitance increased to 106.7, 120.3, and 226.1 F g^{-1} with ECNFs/PtNPs-1, ECNFs/PtNPs-2, and ECNFs/PtNPs-3, respectively, corresponding to Pt loading 10 wt%, 40 wt% and 110 wt%. This is up to 50-fold increase in specific capacitance. It is noteworthy that the specific capacitance of the ECNFs/PtNPs-3 electrode material outperformed the most recent reports using ECNFs based electrode material for supercapacitors [[19], [20], [21], [22]].

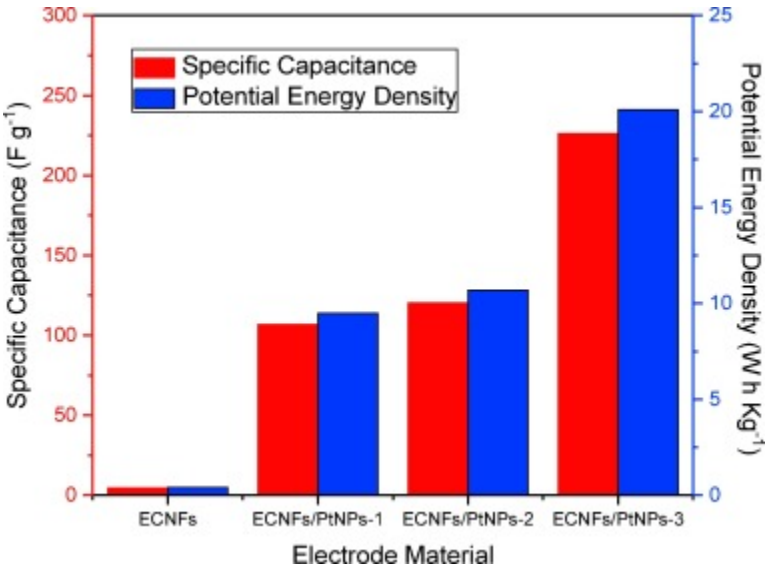

Fig. 4. Comparison charts of specific capacitances and potential energy density of ECNFs and ECNFs/PtNPs electrode materials.

To further compare and evaluate the electrochemical performance of ECNFs and ECNFs/PtNPs electrode materials in supercapacitor application, potential energy density of these electrode materials was calculated by using the following equation (2)

$$E = \frac{1}{2}C(V_c - V_a)^2 \quad (2)$$

where C is the specific capacitance from (1); and V_c–V_a is the sweeping potential window.

The potential energy densities of the ECNF and ECNF/PtNPs electrode materials also increased significantly with Pt loading. Pristine ECNFs possessed a potential energy density of 0.4 W h kg^{-1} while the potential energy density of ECNFs/PtNPs-3 reached 20.1 W h kg^{-1}, another 50-fold increase.

Long-term cycling performance is a crucial parameter for electrode material of supercapacitor. The stability of capacitance performance of the ECNFs/PtNPs-3 electrode material was investigated through galvanostatic charge/discharge test for 2,500 cycles within a potential window from −0.5 V and 0.3 V at a high constant current density of 4,320 mA g^{-1} (Fig. 5). The gravimetric capacitance was merely reduced by 4% after 2,500 cycles of charge/discharge, indicating that the ECNFs/PtNPs-3 electrode material was electrochemical stable and durable.

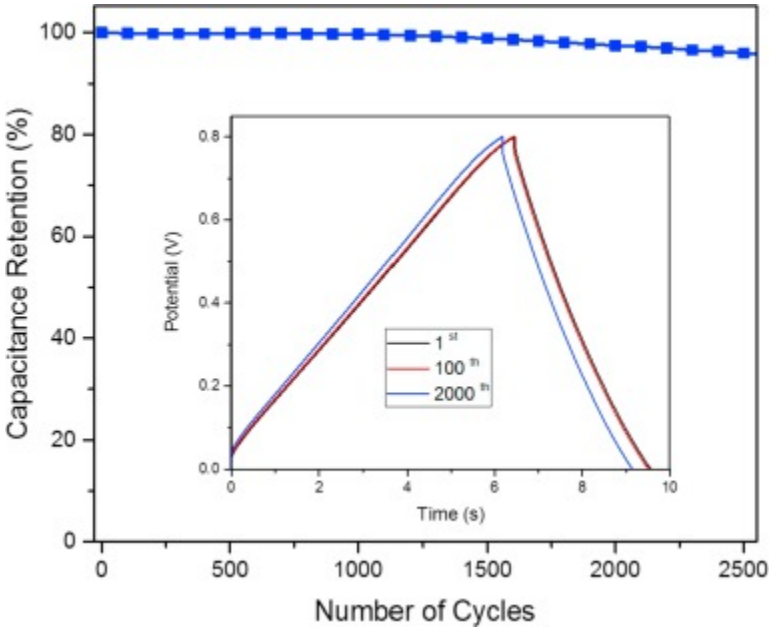

Fig. 5. Cycling stability of ECNFs/PtNPs-3 electrode material under current density of 4320 mA g^{-1} with embedded charge/discharge curves of the 1st, 100^{th}, and 2000^{th} cycles.

3.3. Electrochemical mechanism discussion

The tremendous increase in specific capacitance of the ECNFs/PtNPs electrode materials should not be just due to the increase in specific surface area of the electrode materials. The specific surface area increased by only 54% for ECNFs/PtNPs-3 as compared to the pristine ECNFs but the resultant specific capacitance increased by almost 50 times. Q. Zhang et al. decorated graphene with Pt nanoparticles through one-step γ-ray induced reduction of graphene oxide and chloroplatinic acid and demonstrated that this material possessed higher specific capacitance and better retention rate as supercapacitor electrode than those of undecorated counterpart [17]. Dacheng Zhang et al. revealed that the supercapacitor based on graphene/Pt films showed high rate capability and cyclability [18]. Both of the research work broadly attributed the enhancement of electrochemical performance to accelerated electron transfer and increased electrochemical active surface area caused by Pt nanoparticles. However, detailed mechanism for performance enhancement is still unknown.

In this research, further investigation on the reason for great improvement in specific capacitance with ECNFs/PtNPs electrode material was conducted. From the CV curves in Fig. 3, there were undoubtedly some sort of redox reaction occurred. It is well known that redox reaction can introduce charge transfer between electrode and electrolyte and lead to psuedocapacitance. Hence corresponding increase in specific capacitance of the ECNFs/PtNPs electrode material over the pristine ECNFs electrode material should be attributed to the redox reaction between ECNFs/PtNPs electrode and KOH aqueous electrolyte. Pt based materials are the most practical catalysts for oxygen reduction reaction (ORR) [23] and electro-catalytic ORR reaction is likely to happen in 6M KOH aqueous solution in the presence of PtNPs. To check if the redox reaction that occurred between ECNFs/PtNPs electrode and KOH aqueous electrolyte was related to ORR or not, CV tests were performed at scan rate of 5 mV s^{-1} with ECNFs/PtNPs-3 electrode material using (1) the same 6M KOH aqueous solution but bubbled with continuous N_2 flow; (2) an organic electrolyte of tetraethylammonium tetrafluoroborate ($TEABF_4$) in acetonitrile. As shown in Fig. 6, the CV curve with $TEABF_4$ electrolyte did not show any observable redox peaks while CV curves from both the N_2 bubbled and non-bubbled KOH aqueous electrolytes exhibited significant reduction peaks at −0.317 V and −0.331 V (vs. Ag/AgCl/KCl(3M)), respectively. The current density with N_2 bubbled KOH aqueous electrolyte was slightly smaller than that with non-bubbled KOH aqueous electrolyte (0.992 A g^{-1} vs. 1.062 A g^{-1}). This finding indicated that the redox reaction herein is definitely related to oxygen.

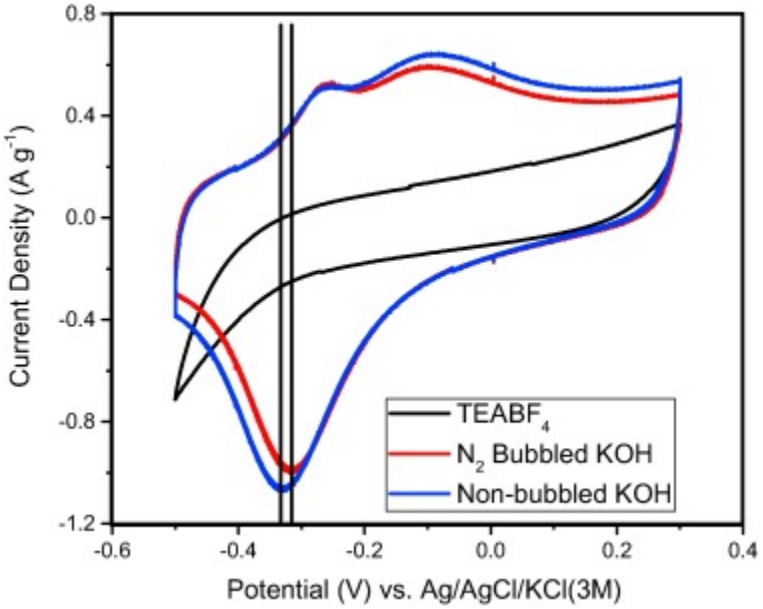

Fig. 6. CV of ECNFs/PtNPs-3 electrode material in different electrolytes at a scan rate of 5 mV s^{-1}.

It is known that the ORR is one of the important reaction in energy converting systems such as fuel cells [24]. Previous studies have demonstrated that the ORR could go with two schemes [24,25]: one could be “direct” 4e reduction and the other could be “series” 4e reduction, which depend on electrode and electrolyte that are involved. W. Jin et al. compared ORR reaction at interface between a polycrystalline Pt solid electrode and NaOH/KOH aqueous solutions with concentrations ranging from 0.5 M to 14 M by cyclic voltammetry and provided further information regarding the mechanism of ORR in alkaline solutions [25]. According to their

research, the ORR occurred at −0.234 V (vs. standard hydrogen electrode (SHE)) on Pt solid surface in 6M KOH aqueous solution with scan rate of 100 mV s^{-1}. It is also reported in the same research that the electron transfer number of the ORR in KOH aquesous solution transitioned from 2 in dilute solution to 1 in 6M solution. Herein the reduction peak occurred at −0.421 V (vs. Ag/AgCl/KCl(3M)) for ECNFs/PtNPs-3 at 100 mV s^{-1} in 6M KOH aqueous solution. It is known that Ag/AgCl/KCl(3M) reference electrode has a potential of approximately 0.210 V versus SHE. The reduction peak at −0.421 V versus Ag/AgCl/KCl(3M) is equivalent to −0.211 V versus SHE, which is close to the reported −0.234 V versus SHE. The reduction reaction in this research, therefore, should be the ORR. The slight reduction peak difference is probably caused by ultra-high specific surface area of PtNPs on ECNFs compared to Pt solid electrode, which could facilitate ORR through larger amount of active sites and enable it at more positive potential. In concentrated KOH aqueous solution, oxygen solubility is very small and solution viscosity is high [25]. Thus N_2 bubbling did not affect oxygen solubility significantly but a slight reduction of amount of oxygen. Therefore a slight ORR current density reduction, from 1.062 A g^{-1} to 0.992 A g^{-1}, was observed for ECNFs/PtNPs-3 electrode material with N_2 bubbling when compared to that in the case without N_2 bubbling. There was also a slight positive shift of ORR peak with N_2 bubbling for the same electrode. This might be caused by slightly less PtOH formation under this condition while formation of PtOH inhibits the oxygen reduction[25].

Based on the abovementioned result and discussion, ECNFs/PtNPs is undoubtedly an effective electrode material to get high specific capacitance with alkali aqueous electrolyte. The uniform distribution of PtNPs on ECNFs surface can effectively catalyze ORR reaction with the 6M KOH aqueous electrolyte more likely through 1e pathway (equation (3)) than 2e pathway (equation (4)) and enable large pseudo-capacitance of the electrode material.

$$O_2 + e^- \rightarrow O_2^- \tag{3}$$

$$O_2 + H_2O + 2e^- \rightarrow HO_2^- + OH^- \tag{4}$$

This pseudo-capacitance couples with electric double layer capacitance from the large surface area of the ECNFs/PtNPs electrode material and significantly increases its overall electrochemical performance in supercapacitor application.

4. Conclusion

A hierarchical carbon composite nanofibrous material (ECNFs/PtNPs) was prepared by electrospinning polyacrylonitrile and subsequent stabilization and carbonization followed by controlled growth of Pt nanoparticles on the electrospun carbon nanofiber (ECNFs) surface through a redox reaction. Three ECNFs/PtNPs samples, denoted as ECNFs/PtNPs-1, ECNFs/PtNPs-2, and ECNFs/PtNPs-3, respectively, were prepared with corresponding Pt loading of 10 wt%, 40 wt% and 110 wt% with respect to ECNFs weight. The acquired ECNFs/PtNPs showed a hierarchical nanostructure, i.e. both individual and agglomerate of PtNPs in the range of tens to hundreds of nanometers homogeneously distributed on surface of ~300 nm carbon nanofibers. The ECNFs/PtNPs was explored as electrode material for supercapacitor application with alkali aqueous electrolyte. The specific capacitance of ECNFs electrode material significantly increased as PtNPs were introduced on ECNFs nanofiber surface

and increased from 4.6 F g^{-1} to 226.1 F g^{-1} with ECNFs/PtNPs-3, which is approximately 50-fold increase. Potential energy density of the ECNFs/PtNPs electrode material also increased significantly from 0.4 W h kg^{-1} with pristine ECNFs to 20.1 W h kg^{-1} with ECNFs/PtNPs-3, another 50-fold increase. Meanwhile the ECNFs/PtNPs electrode material also demonstrated great electrochemical stability and durability. The specific capacitance of ECNFs/PtNPs-3 was merely reduced by 4% after 2,500 cycles of charge/discharge. The large specific capacitance of ECNFs/PtNPs electrode material with alkali aqueous electrolyte was attributed to oxygen reduction reaction in alkali aqueous media that were effectively catalyzed by the PtNPs in the unique hierarchical nanostructure, which enabled large pseudo-capacitance of ECNFs/PtNPs and thus significantly increased its overall specific capacitance. The results herein indicated that the ECNFs/PtNPs carbon composite nanomaterial has a great potential as electrode material for high-performance supercapacitors using aqueous electrolyte.

Acknowledgement

This work was performed at the Joint School of Nanoscience and Nanoengineering of North Carolina A&T State University, a member of Southeastern Nanotechnology Infrastructure Corridor (SENIC) and National Nanotechnology Coordinated Infrastructure (NNCI), which is supported by the National Science Foundation (ECCS-1542174).

References

[1] M. Vangari, T. Pryor, L. Jiang, Supercapacitors: review of materials and fabrication methods, J. Energy Eng. 139 (2012) 72-79.

[2] A. Burke, Ultracapacitors: why, how, and where is the technology, J. Power Sources 91 (2000) 37-50.

[3] R. Kötz, M. Carlen, Principles and applications of electrochemical capacitors, Electrochim. Acta 45 (2000) 2483e-498.

[4] P. Simon, Y. Gogotsi, Materials for electrochemical capacitors, Nat. Mater. 7 (2008) 845-854.

[5] B. Conway, V. Birss, J. Wojtowicz, The role and utilization of pseudocapacitance for energy storage by supercapacitors, J. Power Sources 66 (1997) 1-14.

[6] B.E. Conway, Transition from “supercapacitor” to “battery” behavior in electrochemical energy storage, J. Electrochem. Soc. 138 (1991) 1539-1548.

[7] A. Gonzalez, E. Goikolea, J.A. Barrena, R. Mysyk, Review on supercapacitors: technologies and materials, Renew. Sustain. Energy Rev. 58 (2016) 1189-1206.

[8] S. Chen, J. Zhu, X. Wu, Q. Han, X. Wang, Graphene oxide– MnO2 nanocomposites for supercapacitors, ACS Nano 4 (2010) 2822-2830.

[9] W. Chen, R. Rakhi, L. Hu, X. Xie, Y. Cui, H. Alshareef, High-performance nanostructured supercapacitors on a sponge, Nano Lett. 11 (2011) 5165-5172.

[10] L. Zhang, A. Aboagye, A. Kelkar, C. Lai, H. Fong, A review: carbon nanofibers from electrospun polyacrylonitrile and their applications, J. Mater. Sci. 49 (2014) 463-480.

[11] C. Lai, Z. Zhou, L. Zhang, X. Wang, Q. Zhou, Y. Zhao, et al., Free-standing and mechanically flexible mats consisting of electrospun carbon nanofibers made from a natural product of alkali lignin as binder-free electrodes for high-performance supercapacitors, J. Power Sources 247 (2014) 134-141.

[12] B. Zhang, F. Kang, J.-M. Tarascon, J.-K. Kim, Recent advances in electropsun carbon nanofibers and their application in electrochemical energy storage, Prog. Mater. Sci. 76 (2016) 319-380.

[13] Z. Tai, X. Yan, J. Lang, Q. Xue, Enhancement of capacitance performance of flexible carbon nanofiber paper by adding graphene nanosheets, J. Power Sources 199 (2012) 373-378.

[14] Z. Zhou, X.-F. Wu, Graphene-beaded carbon nanofibers for use in supercapacitor electrodes: synthesis and electrochemical characterization, J. Power Sources 222 (2013) 410-416.

[15] M. Zhi, C. Xiang, J. Li, M. Li, N. Wu, Nanostructured carbon-metal oxide composite electrodes for supercapacitors: a review, Nanoscale 5 (2013) 72-88.

[16] A. Aboagye, H. Elbohy, A.D. Kelkar, Q. Qiao, J. Zai, X. Qian, et al., Electrospun carbon nanofibers with surface-attached platinum nanoparticles as cost-effective and efficient counter electrode for dye-sensitized solar cells, Nano Energy 11 (2015) 550-556.

[17] Q. Zhang, Y. Zhang, Z. Gao, H.-L. Ma, S. Wang, J. Peng, et al., A facile synthesis of platinum nanoparticle decorated graphene by one-step g-ray induced reduction for high rate supercapacitors, J. Mater. Chem. C 1 (2013) 321-328.

[18] D. Zhang, X. Zhang, Y. Chen, C. Wang, Y. Ma, H. Dong, et al., Supercapacitor electrodes with especially high rate capability and cyclability based on a novel Pt nanosphere and cysteine-generated graphene, Phys. Chem. Chem. Phys. 14 (2012) 10899-10903.

[19] W. Nan, Y. Zhao, Y. Ding, A.R. Shende, H. Fong, R.V. Shende, Mechanically flexible electrospun carbon nanofiber mats derived from biochar and polyacrylonitrile, Mater. Lett. 205 (2017) 206-210.

[20] Z. Zeng, Y. Liu, W. Zhang, H. Chevva, J. Wei, Improved supercapacitor performance of MnO2-electrospun nanofibers electrodes by mT magnetic field, J. Power Source 358 (2017) 22-28.

[21] E. Ismar, T. Karazehir, M. Ates, A.S. Sarac, Electrospun carbon nanofiber web electrode: supercapacitor behavior in various electrolytes, J. Appl. Polym. Sci. 135 (2018) 45723.

[22] J. Ding, H.-P. Zhang, X. Li, Y. Tang, G. Yang, Crosslinked carbon nanofiber films with hierarchical pores as flexible electrodes for high performance supercapacitors, Mater. Des. 141 (2018) 17-25.

[23] C. Song, J. Zhang, Electrocatalytic oxygen reduction reaction, in: J. Zhang (Ed.), PEM Fuel Cell Electrocatalysts and Catalyst Layers: Fundaments and Applications, Springer, 2008, pp. 89-134.

[24] R. Jäger, E. Härk, P. Kasatkin, E. Lust, Investigation of a carbon-supported Pt electrode for oxygen reduction reaction in 0.1 M KOH aqueous solution, J. Electrochem. Soc. 161 (2014) F861-F867.

[25] W. Jin, H. Du, S. Zheng, H. Xu, Y. Zhang, Comparison of the oxygen reduction reaction between NaOH and KOH solutions on a Pt electrode: the electrolyte-dependent effect, J. Phys. Chem. B 114 (2010) 6542-6548.